Fluctuation and Noise Letters
Vol. 6, No. 4 (2006) L415–L425

World Scientific
www.worldscientific.com

MURMURS AND NOISE CAUSED BY ARTERIAL NARROWING – THEORY AND CLINICAL PRACTICE

MARTIN BIER
Department of Physics
East Carolina University, Greenville, NC 27858, USA

ORVILLE W. DAY
Department of Physics
East Carolina University, Greenville, NC 27858, USA

DAVID W. PRAVICA
Department of Mathematics
East Carolina University, Greenville, NC 27858, USA

Received 19 July 2006
Revised 6 August 2006
Accepted 11 August 2006
Communicated by Bela Suki

Arterial narrowing can cause an audible whirling in the blood flow. We propose diagnosing such narrowing by simply recording that sound and analyzing its spectrum. We show how the Navier-Stokes equation for flow through a narrowing can be turned into a Schrödinger type equation. The complex eigenvalues of the latter equation give the frequencies and decay rates of the vortices present in the whirling pattern. Our diagnosis is based on understanding the relation between features in the sound spectrum and the severity of the narrowing. Today the most commonly used method of diagnosis is duplex ultrasound. In a small clinical trial our method appears to be as good as duplex ultrasound.

Keywords: Arterial stenosis; blood flow; Kolmogorov cascade; vortex dynamics.

1. Introduction

When blood flows through a narrowing (sometimes called a "stenosis") in an artery, a murmur can arise. In the medical literature such an arterial murmur is often termed a "bruit" (BROO'e). If the frequency is sufficiently high, bruits can be heard with a stethoscope. Cardiac physiologists have been aware for centuries that stenoses can form a serious health hazard. They are particularly dangerous in the aorta and in the left and right neck (or carotid) arteries that branch off from the aorta about 10 cm away from the heart. When severe narrowings are suspected

the general medical strategy is to measure the arterial blood speed at five different points with duplex ultrasound [1]. Normally the arterial blood speed amounts to about 0.5 m/s. Using ultrasound equipment, nonuniformities in the blood flow can be picked up through the Doppler effect. It is these nonuniformities that are the indicators of the presence of a stenosis. The medical decision whether to take invasive action or not is generally based on ultrasound diagnosis. However, ultrasound diagnosis may be incomplete as some stenoses may not be picked up with just five measurement points. It, furthermore, requires a skilled technician to properly align the measurement probe with the arterial direction. Ultrasound imaging is also time consuming and the involved equipment is large and very expensive. Below we will show how we record arterial noises in the infrasound regime with three microphones in a girdle (see Fig. 1). We process the ensuing frequency spectra of the sound to diagnose for possible problems. We will show how we have solved the inverse problem that leads us from these induced sound spectra back to the severity of the stenosis.

Fig. 1. A "hooked-up" patient together with the equipment to process the data. The girdle contains three microphones. Two microphones are pressed against left and right artery in the neck. One microphone is pressed against the heart region. Power spectra for the 1–40 Hz regime are taken from all three microphones and checked for the signs of arterial narrowing.

We start, in Sec. 2, with a description, in terms of the Navier-Stokes equation, of how a narrowing in a fluid-flow-tube gives rise to traveling vortices with a very discrete set of frequencies. The mathematical analysis is intricate and readers with a differently focussed interest can turn immediately to Sec. 3 in which we interpret the derived spectrum and compare the analytical results with numerical simulations of the Navier-Stokes equations. In Sec. 4 we compare these results with spectra derived from our infrasound recordings. Finally, in the same section, we show the results of a clinical trial in which we compared the efficacy of our infrasound diagnosis with the results of the customary ultrasound diagnosis.

2. Turning the Navier-Stokes Equation into a Schrödinger Equation

Blood flow is powered by an oscillating pressure that is generated in the heart. In Refs. [2–4] it is shown that, for the flow of blood in the aorta and in the neck arteries, this oscillating pressure leads to a plug-like flow front. The human aorta is about

3 cm in diameter. Only at the aortic wall is there a layer of a few millimeters thick in which the velocity varies from zero at the wall to the plug speed [2]. We idealize the blood flow in the sense that we assume the blood to be a Newtonian fluid between inflexible arterial walls that moves toward the stenosis at constant uniform speed under constant pressure. There are experimental data to support these assumptions [4]. To analyze what happens when plug-like flow is forced through a narrowing, we turn to the Navier-Stokes equations [5] for flow of incompressible (ρ is constant) fluid:

$$\partial_t \vec{u} + \tilde{u} \cdot \tilde{\nabla} \vec{u} = -\rho^{-1} \nabla P + \nu_0 \Delta \vec{u}\,, \tag{1}$$

where $\vec{u}$ represents the velocity field of the flow. The left hand side represents an acceleration operator. $\tilde{u} \cdot \tilde{\nabla} \vec{u}$ is an inertial term that, with $\vec{u} = u_x \vec{i} + u_y \vec{j} + u_z \vec{k}$, can be written as $(u_x \partial_x + u_y \partial_y + u_z \partial_z)\vec{u}$. The physical meaning of this latter term can be better intuited if we write it as $P_{\vec{u}}(\frac{1}{2}\nabla \|\vec{u}\|^2)$, where $P_{\vec{u}}$ stands for the projection on $\vec{u}$. Then $\tilde{u} \cdot \tilde{\nabla} \vec{u}$ is clearly recognized as the $\vec{u}$-component of the gradient of a kinetic energy, i.e. a force. The first term on the right hand side stands for a pressure gradient. The second term on the right hand side stands for the frictional loss of energy and carries the kinematic viscosity ν_0 as a proportionality factor. We, furthermore, have div $\vec{u} = 0$ since the flow is source free and the fluid is incompressible.

We will describe 2D flow in the xy-plane and assume axial symmetry around a line through the center of the artery. Technically, we should convert to cylindrical coordinates. However, in the eventual perturbation analysis the effect of the "cylindricality" only enters at second order. Our analysis will be limited to first order effects and coordinate change is therefore not needed. By virtue of $\mathrm{div}\,\vec{u} = 0$ we can express $\vec{u}$ as the curl of a stream function $\psi(x, y)$, i.e. $\vec{u} = -\mathrm{curl}(\psi \vec{k})$, where $\vec{k}$ is a unit vector in the z-direction. This implies for the components of the velocity field: $u_x = -\partial_y \psi$ and $u_y = \partial_x \psi$. If one imagines a small leaf floating on the fluid in the xy-plane, then the angular speed of this piece of paper is proportional to the norm of the vector $\omega(x, y)\vec{k} = \mathrm{curl}\vec{u}$. Eventually, we have a scalar equation $\omega = -(\mathrm{curl}\ \mathrm{curl}(\psi \vec{k})) \cdot \vec{k} = \Delta\psi$, where Δ represents the Laplace operator, i.e. $\Delta = \partial_x^2 + \partial_y^2$. Because of the aforementioned plug-like nature, blood flow is dominated by an irrotational background flow $\psi_0 = -U_0 y$. Due to initial conditions, boundary effects and the geometry of the stenosis we get a small rotational component $\omega(x, y, t)$ that we will treat as a pertubation:

$$\psi(x, y, t) = \psi_0(x, y) + \psi_1(x, y, t). \tag{2}$$

The stream function ψ_1 can ultimately be found from the vorticity ω by solving Poisson's equation, i.e. $\Delta\psi_1 = \omega$ with appropriate boundary conditions. By taking the curl of both sides of Eq. (1), we remove the pressure gradient term (the pressure can be reobtained by taking the divergence on both sides of Eq. (1) and solving the ensuing Poisson's equation). We then get:

$$\partial_t \omega + \frac{\partial(\psi, \omega)}{\partial(x, y)} = \nu_0 \Delta\omega, \tag{3}$$

where the "Advection of Vorticity" term is defined as

$$\frac{\partial(\psi,\omega)}{\partial(x,y)} = \partial_x\psi\partial_y\omega - \partial_y\psi\partial_x\omega = u_x\partial_x\omega + u_y\partial_y\omega = \vec{u}\cdot\text{grad }\omega. \tag{4}$$

Navier-Stokes equations are notoriously hard and fluid flow through a narrowing or around an obstacle is not generally accessible for analytic evaluation. Researchers have therefore commonly resorted to numerical simulation [6]. The rare instances that allow for some "analytic access" are those where the obstacle or narrowing can be described by a conformal mapping. A conformal map is an isomorphism that can be expressed as an analytic function $\zeta(z)$ from $z = x + iy \in \mathbf{C}$ to $\zeta = \xi + i\eta \in \mathbf{C}$. To see how effective such a map can be,consider the Joukowski transformation $\zeta = z + 1/z$ (which leads to $\xi = x + x/(x^2+y^2)$ and $\eta = y - y/(x^2+y^2)$). It is easy to see that the curves for $\eta = constant$ correspond to a unit circle and what looks like smooth streamlines around this circle. Such streamlines constitute a natural zeroth order starting point for a perturbation analysis [3].

For a narrowing in an artery an appropriate transformation is

$$\zeta(z) = \frac{z}{h}\exp\left[-\frac{m}{1+z^2/p^2}\right], \tag{5}$$

where h is the half width of the tube, m is a dimensionless measure for the depth of the stenosis into the tube, and p is a measure for the width of the stenosis. A pure Gaussian inserted in the interior of the tube may be mathematically simpler at first sight. However, such a shape does not correspond to a simple conformal map and numerical simulation is ultimately the only possible venue of investigation in that case [6]. In the coordinates ξ and η Eq. (3) is rewritten as:

$$\partial_t\omega + J(\zeta;z)\frac{\partial(\psi,\omega)}{\partial(\xi,\eta)} = \nu_0 J(\zeta;z)\Delta_{\xi,\eta}\omega\,, \tag{6}$$

where $\Delta_{\xi,\eta} = \partial_\xi^2 + \partial_\eta^2$ and $J(\zeta;z)$ denotes the Jacobian

$$J(\zeta;z) \equiv \frac{\partial(\xi,\eta)}{\partial(x,y)} = \left|\frac{\partial\zeta}{\partial z}\right|^2. \tag{7}$$

For a vorticity equation like Eq. (6), a logical substitution is $\omega(\xi,\eta,t) = \exp[i\nu_0\lambda t]$ $\exp[\beta R_0\xi]W(\xi,\eta)$. The idea behind this substitution is very similar to that of the well known WKB approximation. With $\exp[i\nu_0\lambda t]$ we assume a harmonic time dependence. $W(\xi,\eta)$ denotes the vorticity amplitude. The factor $\exp[\beta R_0\xi]$ makes terms cancel in the differential equation that ensues from Eq. (6); $\exp[\beta R_0\xi]$ essentially symmetrizes the downstream and the upstream part of the flow relative to the narrowing or obstacle. $R_0 = U_0 h/\nu_0$ is the Reynolds number constructed from the average flow speed U_0, the scale h of the obstacle or narrowing (it would be unity in case of the aforementioned unit circle and the Joukowski transformation), and the kinematic viscosity ν_0. β is a positive real number and it depends on the specifics of the setup what value of β results in the required cancellation. Substituting the uniform irrotational background flow $\psi_0(\xi,\eta) = -U_0 h\eta(x,y)$ for ψ in Eq. (6) we

obtain an equation for the vorticity amplitude W:

$$-\Delta_{\xi,\eta} W + \left(\frac{i\lambda}{J}\right) W = -\left(\frac{R_0}{2}\right)^2 W \tag{8}$$

After solving for W, both the vorticity ω and the rotational part of the flow ψ_1 can be found. Because we substituted ψ_0 in Eq. (6), we have with ψ_1 a rotational flow that constitutes a perturbation on the irrotational background flow. Equation (8) is a Schrödinger-type equation: the coefficient of the second W term on the left hand side can be interpreted as a potential (J depends on ζ), and the coefficient of W on the right hand side acts like an eigenvalue. We reorganize Eq. (8) and work with a potential $V_r(\xi,\eta) \equiv 1/J - h^2 \exp[-m]$. We then have a V_r that, at the origin, is quadratic in ξ and η. We next reformulate Eq. (8) and see whether V_r supports resonant states in the quantum mechanical sense [8]. With $\mu^2 = -i\lambda h^2 \exp[-2|m|]$ as a parameter that couples the potential V_r to the eigenvalue we have:

$$-\Delta_{\xi,\eta} W - \mu^2 V_r(\xi,\eta) W = -\left[\mu^2 + \left(\frac{R_0}{2}\right)^2\right] W\,. \tag{9}$$

In the potential V_r there is a saddle at $(\xi,\eta) = (0,0)$; the maximum is in the flow direction ξ. It is only after complex scaling, i.e. $\xi \to e^{\theta}\xi$ for a specific complex θ [7,8], that we obtain square solutions and a potential that has a minimum at the origin. We can then work with ordinary solutions of the Schrödinger equation for the harmonic oscillator as approximate solutions. Because of the complex scaling the eigenvalues, $E = -\left[\mu^2 + (\frac{R_0}{2})^2\right]$, turn out to be complex.

Note that a bound state must have a positive value for μ^2. That leads to a negative real value for $i\lambda$ and this means that the accompanying eigensolution does not oscillate, but, instead, decays over time. Only complex values for $i\lambda$ lead to oscillations.

Figure 2 shows a set of complex eigenvalues obtained for physiologically realistic parameter values. For a more detailed description of the exact mathematical derivation of these eigenvalues we refer to [7].

3. The Interpretation of the Schrödinger-Vorticity Equation

The spectrum of complex eigenvalues depicted in Fig. 2 is the result of the mathematical tour de force presented in Sec. 2. It is the physical interpretation of this spectrum that we will discuss in this section. For every point in Fig. 2, the vertical coordinate represents a frequency and the horizontal coordinate represents a decay rate. In [7] we established the physical reality of the lowest frequency in Fig. 2. The plug speed U_0 of the liquid divided by the length of the stenosis (the parameter p) constitutes a characteristic frequency, f_0, of the system. If we let f_1 be the lowest frequency present in the downstream whirling pattern, then f_1/f_0 defines the so-called Strouhal number [5]. Because the Navier-Stokes equations are so hard to treat analytically, engineers commonly limit their efforts to an experimental determination of the Strouhal number. The Strouhal number that derives from the lowest frequency in Fig. 2 corresponds well with experimentally measured ones.

In 1941 Kolmogorov proposed the following model for turbulence. Vortices would initially be generated at large size and low frequency. These vortices would next

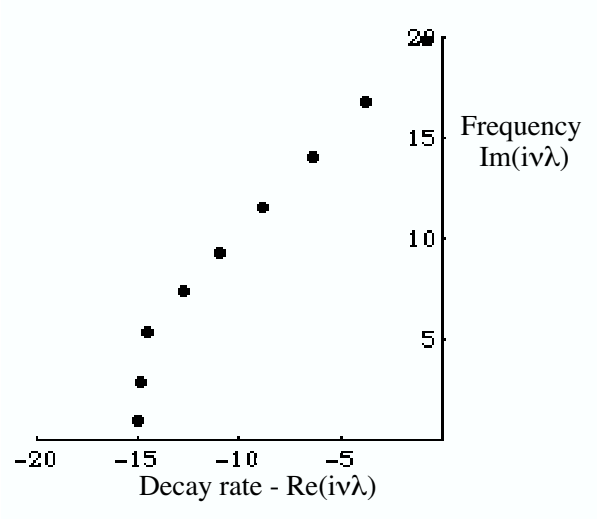

Fig. 2. Spectrum of complex eigenvalues for width and depth characteristics of the stenosis of $p = 0.02$ and $m = -0.5$ (see text for the exact meaning p and m). The Reynolds number is taken to be $R_0 = hU_0/\nu_0 = 2000$. Such a Reynolds number would correspond to a blood speed of $U_0 = 0.4$ m/s, an aortic diameter of 0.03 m, and a kinematic viscosity of the blood of $\nu_0 = 3.0 \times 10^{-6}$ m^2/s. The horizontal coordinates of the points making up the spectrum correspond to decay rates. The vertical coordinates correspond to frequencies.

pass on their energy to faster smaller-sized vortices. A cascade proceeds to ever smaller sizes and ever higher frequencies [9]. As the length scale of the vortices decreases, so does the Reynolds number. The last and fastest vortices occur when the Reynolds number is about one. It is through dissipation that the energy of these submillimeter sized vortices then finally turns into heat.

Kolmogorov's turbulence is isotropic. It is also steady state in the sense that the flow of energy down the cascade of vortices is constant. The situation with our stenosis is somewhat different. Our Reynolds number is such that we are still far away from full fledged turbulence. Unlike Kolmogorov's case, we operate in a 2D regime that is still amenable to treatment in terms of perturbation analysis; the vortices that we describe are perturbations that occur inside the "plug" as it is forced through the stenosis. The ultimate behavior of our system is similar to that in a well known Von Karman vortex street [5]. When fluid flows around a cylinder (a case in which the aforementioned Joukowski transformation applies) a periodic "shedding" of vortices from the downstream side of the cylinder can occur. The shedding frequency is commonly taken as the aforementioned Strouhal frequency f_1. As these shedded vortices flow downstream away from the cylinder, they break up into smaller faster vortices very much like in a Kolmogorov cascade. Vortex shedding is also what occurs with a narrowing in a tube.

Going to Fig. 2 we assume that a big vortex U_1 of frequency f_1 is created at the stenosis. This vortex passes on its energy at a rate k_1 to U_2. U_2 represents vortices of frequency f_2. The energy in U_2 is passed on to U_3 at a rate k_2, etc. It is from U_9 that energy is finally dissipated into heat (cf. Fig. 3). The distribution

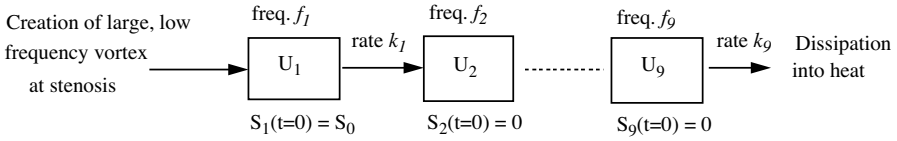

Fig. 3. Markov chain model for the whirling, downstream from the stenosis. At $t = 0$ a large vortex of the lowest frequency, f_1, forms at the stenosis. This vortex passes on its energy at a rate k_1 to vortices of frequency f_2, etc. As the energy passes through the chain, vortices are carried downstream at the same time. Substituting the 9 frequencies and rates depicted in Fig. 2 leads to the power spectra depicted in Fig. 4(a).

of energy over these 9 frequencies constitutes a power spectrum; a power spectrum that changes with time. Because of the uniform flow in which the vortex dynamics is embedded, we should see the evolution of the spectrum as we look further and further downstream.

The system depicted in Fig. 3 is a Markov chain. Chains like these are frequently encountered in the applied sciences. Radioactive decay cascades, for instance, are modeled by chains of exactly the form of Fig. 3. In its Sec. 6.2, the well known textbook by Bharucha-Reid [10] presents an exact solution for a cascade that starts with $S_1(0) = S_0$ and $S_i(t) = 0$ for $i \neq 1$:

$$S_i(t) = S_0 \sum_{j=1}^{i} \alpha_{ij} \exp[-k_j t] \text{ , with } \quad \alpha_{ij} = \frac{\prod_{m=1}^{i-1} k_m}{\prod_{m=1,\ m\neq j}^{i} (k_m - k_j)} \,. \tag{10}$$

It is straightforward to take the rates from Fig. 2 and substitute them in Eq. (10) to obtain Fig. 4(a). Figure 4(b) shows the results of a numerical simulation of the Navier-Stokes equations. The resemblance of Figs. 4(a) and 4(b) provides support for our interpretation of the eigenvalue spectrum in Fig. 2.

For the initial, large scale, vortices the product of the size l_i and the speed v_i divided by the kinematic viscosity is expected to be of the order of magnitude of the Reynolds number R_0. The final, smallest scale, vortices have size l_f and speed v_f. For these vortices to next be dissipated into heat the Reynolds number should be around unity. So we have $(l_i v_i)/(l_f v_f) \sim R_0$. A dimensional analysis led Kolmogorov to the following distribution of R_0 over size and speed: $l_i/l_f \sim R_0^{3/4}$ and $v_i/v_f \sim R_0^{1/4}$ [9]. The frequencies of the initial and final vortices can be taken as $f_i = v_i/l_i$ and $f_f = v_f/l_f$. We find the ratio f_f/f_i then to be of the order of magnitude of $\sqrt{R_0}$. For the case of Figs. 2, 3, and 4 we have 45 for the value of $\sqrt{R_0}$. This is indeed of the same order of magnitude as f_1/f_9, the ratio of the highest and lowest frequency in Figs. 2 and 3, which turns out to be about 20.

The harmonic oscillator eigenfunctions that give rise to the spectrum in Fig. 2 are valid approximations near the stenosis. What happens downstream is outside the regime where this approximation applies and is, therefore, open to conjecture. The cascade in Fig. 3 and the ensuing result in Fig. 4(a) are not rigorously derived and constitute such a conjecture.

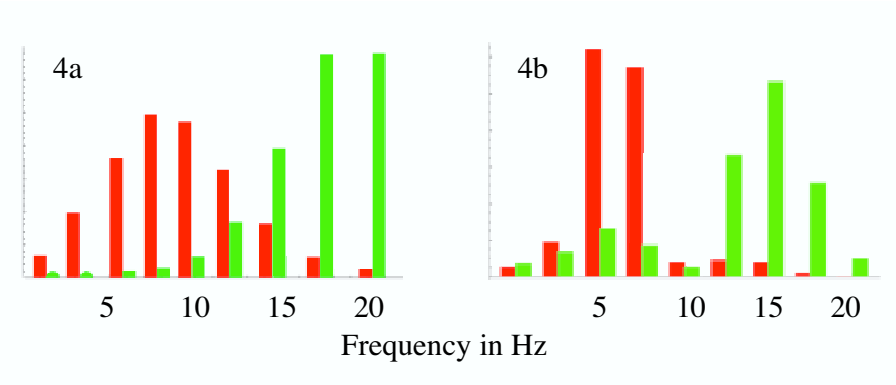

Fig. 4. (a) Power spectra based on the frequencies and rates of Fig. 2 and the mechanism of Fig. 3. The maximum of the spectrum is seen to move from about 7 Hz at $t = 0.25$ s (red) to about 17 Hz at $t = 0.75$ s (green). (b) A numerical simulation of the actual Navier-Stokes equations yields a similar result. To obtain this figure the fluid speed perpendicular to the flow direction was recorded at 0.625 cm from the wall of the virtual artery. The interval between 0 Hz and 20 Hz was divided into equal 9 segments. The height of each bar indicates the power in each segment. Depicted are spectra taken at 0.1 m (red) and 0.3 m (green) downstream from the stenosis. With a blood speed of 0.4 m/s these positions correspond exactly to the times for the spectra in (a).

4. Clinical Application and Clinical Trial

Subjects first underwent an ultrasound examination of the left and right neck arteries. That procedure took between 15 and 20 minutes. After that, they were given a description of our study and required to sign an approval form. Subjects were then fitted with the girdle with the three sensors as depicted in Fig. 1. The subject was asked to breath normally without coughing or moving. After the simultaneous 30 second recording for all three channels, the device was removed. The data were originally recorded at a sampling rate of 44 kHz and stored in a 16 bit WAV file. The ensuing files were subsequently filtered and smoothed to obtain a power spectrum for the 0–40 Hz range (cf. Fig. 5).

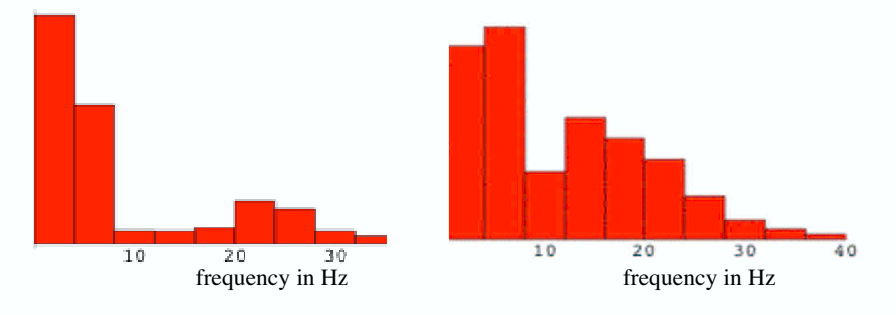

Fig. 5. Infrasound power spectra from a neck artery of a healthy patient (left) and from a patient with an arterial stenosis (right). The peaks at the lowest frequency bins derive from the beating heart. It is the peaks at slightly higher frequencies that are indicators of arterial narrowing.

Signals in the 1–5 Hz regime result mainly from the cardiac cycle. We take the signal from the microphone over the heart region to assess the strength of the cardiac signal. It is with the microphones on the neck arteries that we pick up arterial sounds. Even sound generated in the aorta is easily picked up from the neck arteries. As we showed in Secs. 2 and 3, it is large peaks in the 10–20 Hz range that are associated with arterial narrowing. No peaks, or low peaks with fast fall-off indicate good arterial health. An exact quantitative connection between the patient spectra in Fig. 5 and those in Fig. 4 is hard to make. Figures 4(a) and 4(b) are power spectra for the whirling pattern in the artery at a particular distance from the narrowing. It is attenuated and dispersed sound from different locations along the artery that reaches our microphones. It is, nevertheless, straightforward to write a computer program that uses the patient spectra to evaluate the severity of arterial narrowing. With duplex ultrasound diagnosis it is standard to categorize patients from A to E for increasing severity [1]. In our computer program we first subtract the cardiac signal from the neck artery spectrum (cf. Fig. 5). For the remaining spectrum we then divide the power in the > 5 Hz regime by the total power and use the resulting quotient to classify a patient as A, B, C, D, or E.

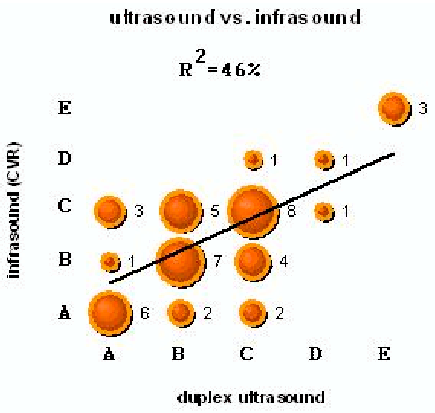

Fig. 6. Scatter chart showing a good agreement between our infrasound method and the customary duplex ultrasound method for diagnosing arterial narrowing. Patients are ranked A to E for increasing stenosis severity. A is completely healthy. E requires immediate medical attention. The circle with the number 4 indicates that 4 patients categorized C by ultrasound were ranked B by our infrasound method. All the E's that were picked up by ultrasound were apparently also picked up by infrasound.

The results of a small clinical trial with 22 patients are plotted in Fig. 6. Forty-four neck arteries, 22 left and 22 right, were subjected to ultrasound diagnosis as well as to our procedure. Our procedure easily identified the three arteries with more than 95% blockage (category E), giving preliminary evidence that our device may be very useful as a screening tool.

5. Discussion

In Secs. 2 and 3 we presented techniques to derive a Schrödinger-type eigenvalue problem from the Navier-Stokes equation and to analyze the ensuing spectrum of

complex eigenvalues. These procedures have not been widely used, but they should, in principle, be applicable to a wide variety of setups and could perhaps be utilized to study the onset of turbulence.

Our perturbation analysis pertains to a very idealized system. There are ignored features and factors that also impinge on the spectra that we ultimately measure through our microphones. However, our theory shows and our clinical work affirms that it is in the infrasound regime, between cardiac frequencies and audible frequencies, that a bigger stenosis leads to a stronger signal.

In our immediate cardiovascular context, the methods and device described in this Letter may be relevant for more ailments than just arterial narrowing. An aneurysm is modeled with a negative value for m in Eq. (5) and a spectrum can be easily evaluated for that case. Another promising possibility is to use our recordings as a noninvasive way to determine the viscosity of blood. Here we would make use of the fact that the frequency spectrum (cf. Fig. 2) depends on the Reynolds number and that the Reynolds depends on viscosity. Increased or decreased viscosity is associated with a number of ailments. More ideas, more clinical trials, and more systematic research into the relation between recorded sound and blood flow are clearly necessary.

Our method to diagnose arterial narrowing appears to be as good as the ultrasound based method. However, our equipment is cheap and easy to handle. The girdle with the microphones and the additional computer program should be orders of magnitude cheaper than ultrasound equipment. An average patient should actually be able to keep our infrasound setup at home and determine for him- or herself in which of the five categories of arterial health he or she falls.

Acknowledgements

We thank Kees van den Doel for his useful feedback. We are, furthermore, very grateful to the patients that volunteered, without remuneration, to be strapped in and have a recording made.

References

[1] J. M. Edwards, G. H. Moneta, G. Papanicolaou *et al.*, Prospective validation of a new duplex ultrasound criteria for 70-99% internal carotid stenosis, *Journal d'échographie et de Médecine par Ultrasons* **16** (1995) 3–7.

[2] Y. C. Fung, *Biodynamics*: *Circulation* (Springer-Verlag, New York, 1984).

[3] C. Pozridikis, *Introduction to Theoretical and Computational Fluid Dynamics* (Oxford University Press, Oxford, 1997).

[4] C. G. Caro, T. J. Pedley, R. C. Schroter and W. A. Seed, *The Mechanics of the Circulation* (Oxford University Press, Oxford, 1978).

[5] G.K. Batchelor, *An Introduction to Fluid Dynamics* (Cambridge University Press, Cambridge, 1967).

[6] W. Liao, T. S. Lee and H. T. Low, Numerical study of physiological turbulence flows through stenosed arteries, *Int. J. Comput. Modern Physics C* **14**(5) (2003) 635–659.

[7] D.W. Pravica, M. Bier, R.S. Brock and O. W. Day, Stable stationary vortices and traveling oscillatory vortices in a stenotic fluid-flow channel *Phys. Rev. E* **72** (2005) 067303-1–067303-4.

[8] P. Briet, J.M. Combes and P. Duclos, On the location of resonances for Schrödinger operators in the semi-classical limit. II, *Commun. Part. Diff. Eq.* **12** 201 (1987).

[9] A. N. Kolmogorov, The local structure of turbulence in incompressible viscous fluids at very large Reynolds numbers, *Dokl. Akad. Nauk. SSSR* **30** (1941) 301–304. [Reprinted in: *Proc. R. Soc. Lond. A*, **434** (1991) 9–13].

[10] A. T. Bharucha-Reid, *Elements of the Theory of Markov Processes and their Applications* (Dover Publications, Mineola, N.Y., 1997).